Supporting Material: A wall-shear-stress based model for adhesive dyanmics of red blood cells in malaria, by *Fedosov et al.*

March 12, 2011

METHODS AND MODELS

Plasmodium falciparum (Pf) parasitized red blood cells (Pf-RBCs) and their external/internal fluids are modeled with the Dissipative Particle Dynamics (DPD) method (1,2).

RBC membrane model

The RBC membrane is constructed by N_v particles $\{x_{i=1...N_v}\}$ which correspond to a two-dimensional triangulated network (3,4) on the RBC surface measured (5) and is given by

$$z = \pm D_0 \sqrt{1 - \frac{4(x^2+y^2)}{D_0^2}} \left[a_0 + a_1 \frac{x^2+y^2}{D_0^2} + a_2 \frac{(x^2+y^2)^2}{D_0^4} \right], \quad (1)$$

where $D_0 = 7.82\ \mu m$ is the average diameter, $a_0 = 0.0518$, $a_1 = 2.0026$, and $a_2 = -4.491$. The surface area and volume of this RBC are equal to 135 μm^2 and 94 μm^3, respectively.

The vertices of the network are connected by N_s springs with the following potential energy

$$V_s = \sum_{j \in 1...N_s} \left[\frac{k_B T l_m (3x_j^2 - 2x_j^3)}{4p(1-x_j)} + \frac{k_p}{(n-1) l_j^{n-1}} \right], \quad (2)$$

where l_j is the length of the spring j, l_m is the maximum spring extension, $x_j = l_j / l_m$, p is the persistence length, $k_B T$ is the energy unit, k_p is the spring constant, and n is a power. The above equation consists of the attractive wormlike chain potential and a repulsive potential for $n > 0$ such that a non-zero equilibrium spring length can be imposed.

Membrane viscosity is incorporated into the RBC model through a dissipative force for each spring. The general framework of the fluid particle model (6) allows us to define dissipative $\mathbf{F}_{ij}^D$ and random $\mathbf{F}_{ij}^R$ forces, which satisfy the fluctuation-dissipation balance providing consistent temperature of the RBC membrane in equilibrium. The forces are as follows

$$\mathbf{F}_{ij}^D = -\gamma^T \mathbf{v}_{ij} - \gamma^C (\mathbf{v}_{ij} \cdot \mathbf{e}_{ij}) \mathbf{e}_{ij}, \quad (3)$$

$$\mathbf{F}_{ij}^R dt = \sqrt{2 k_B T} \left(\sqrt{2\gamma^T}\, d\overline{\mathbf{W}_{ij}^S} + \sqrt{3\gamma^C - \gamma^T}\, \frac{tr[d\mathbf{W}_{ij}]}{3} 1 \right) \cdot \mathbf{e}_{ij}, \quad (4)$$

where γ^T and γ^C are dissipative parameters, v_{ij} is the relative velocity of spring ends, $tr[d\mathbf{W}_{ij}]$ is the trace of a random matrix of independent Wiener increments $d\mathbf{W}_{ij}$, and $d\overline{\mathbf{W}_{ij}^S} = d\mathbf{W}_{ij}^S - tr[d\mathbf{W}_{ij}^S]1/3$ is the traceless symmetric part.

The bending resistance of the RBC membrane is modeled by

$$V_b = \sum_{j \in 1 \ldots N_s} k_b \left[1 - \cos(\theta_j - \theta_0) \right], \tag{5}$$

where k_b is the bending constant, θ_j is the instantaneous angle between two adjacent triangles having the common edge j, and θ_0 is the spontaneous angle.

Moreover, the RBC model requires the area and volume conservation constraints, which mimic area-incompressibility of the lipid bilayer and incompressibility of a cytosol, respectively. Such constraints are imposed as follows

$$V_{a+v} = \sum_{j \in 1 \ldots N_t} \frac{k_d (A_j - A_0)^2}{2A_0} + \frac{k_a (A - A_0^{tot})^2}{2A_0^{tot}} + \frac{k_v (V - V_0^{tot})^2}{2V_0^{tot}}, \tag{6}$$

where N_t is the number of triangles in the membrane network, A_0 is the triangle area, and k_d, k_a and k_v are the local area, global area and volume constraint coefficients, respectively. The terms A and V are the total RBC area and volume, while A_0^{tot} and V_0^{tot} are the specified total area and volume, respectively.

Membrane macroscopic properties

Linear analysis of a regular hexagonal network allows us to uniquely relate the model parameters and the network macroscopic elastic properties (shear, area-compression, and Young's moduli), see (4,7) for details. Thus, the membrane shear modulus is given by

$$\mu_0 = \frac{\sqrt{3} k_B T}{4 p l_m x_0} \left(\frac{x_0}{2(1 - x_0)^3} - \frac{1}{4(1 - x_0)^2} + \frac{1}{4} \right) + \frac{\sqrt{3} k_p (n+1)}{4 l_0^{n+1}}, \tag{7}$$

where l_0 is the equilibrium spring length and $x_0 = l_0 / l_m$. The area-compression K and Young's Y_0 moduli are equal to $2\mu_0 + k_a + k_d$ and $4K\mu_0/(K + \mu_0)$, respectively.

The relation between the model bending coefficient k_b and the macroscopic bending rigidity k_c of the Helfrich model (8) can be derived as $k_b = 2k_c/\sqrt{3}$ for a spherical membrane (4,9). This expression describes bending contribution of the energy in equation (5), but may not fully represent actual bending resistance of the RBC membrane since membrane bending may also result in local in-plane deformations.

The membrane shear viscosity η_m is related to the dissipative parameters γ^T, γ^C as $\eta_m = \sqrt{3}(\gamma^T + \gamma^C/4)$. Here γ^T accounts for a large portion of viscous contribution, and hence γ^C is set to $\gamma^T/3$ in all simulations.

In practice, the given macroscopic RBC properties serve as an input to be used to calculate the necessary mesoscopic model parameters from the equations above without any manual adjustment. A simulation of a RBC in equilibrium shows that the membrane may develop local bumps due to stress anomalies in a membrane triangulation since a network on a closed surface cannot consist of triangles whose edges have the same lengths. Such local stress artifacts depend on the network regularity and the ratio of the membrane elastic and bending contributions given by the Föppl-von Kármán number $\kappa = Y_0 R_0^2 / k_c$, where $R_0 = \sqrt{A_0^{tot}/(4\pi)}$. To eliminate the stress

artifacts we employ a ``*stress-free*'' model obtained by computational annealing. Thus, the equilibrium length l_0^i of each spring is set to the edge length after triangulation for $i = 1,\ldots,N_s$. This results in an individual maximum spring extension $l_m^i = l_0^i \times x_0$ (x_0 is a constant) and the spring parameters calculated for each spring using equation (7) for given μ_0. This modification provides a network free of local stress anomalies.

RBC-solvent boundary conditions

The RBC membrane encloses a volume of fluid and is itself suspended in a solvent. In particle methods, such as DPD, fluids are represented as a collection of interacting particles. Thus, in order to impose appropriate boundary conditions (BCs) between the membrane and the external/internal fluids two matters need to be addressed:

i) enforcement of membrane impenetrability to prevent mixing of the inner and the outer fluids,
ii) no-slip BCs imposed through pairwise point interactions between the fluid particles and the membrane vertices.

Membrane impenetrability is enforced by imposing bounce-back reflection of fluid particles at the moving membrane triangular plaquettes. The bounce-back reflection enhances the no-slip boundary conditions at the membrane surface as compared to specular reflection; however, it does not guarantee no-slip. Additional dissipation enhancement between the fluid and the membrane is required to achieve no-slip at the membrane boundary. For this purpose, the DPD dissipative force between fluid particles and membrane vertices needs to be properly set based on the idealized case of linear shear flow over a flat plate. In continuum, the total shear force exerted by the fluid on the area A is equal to $A\eta\dot{\gamma}$, where η is the fluid's viscosity and $\dot{\gamma}$ is the local wall shear-rate. In DPD, we distribute a number of particles on the wall to mimic the membrane vertices. The force on a single wall particle exerted by the sheared fluid can be found as follows

$$F_v = \int_{V_h} n g(r) F^D dV, \tag{8}$$

where F^D is the DPD dissipative force (6) between fluid particles and membrane vertices, n is the fluid number density, $g(r)$ is the radial distribution function of fluid particles with respect to the wall particles, and V_h is the half sphere volume of fluid above the wall. Here, the total shear force on the area A is equal to $N_A F_v$, where N_A is the number of wall particles enclosed by A. The equality of $N_A F_v = A\eta\dot{\gamma}$ results in an expression of the dissipative force coefficient in terms of the fluid density and viscosity, and the wall density N_A/A, while under the assumption of linear shear flow the shear rate $\dot{\gamma}$ cancels out. This formulation results in satisfaction of the no-slip BCs for the linear shear flow over a flat plate. It also serves as an excellent approximation for no-slip at the membrane surface in spite of the assumptions made. Note that in the absence of conservative interactions between fluid and wall particles $g(r) = 1$.

Adhesion model

Adhesion of Pf-RBCs to coated surfaces is mediated by the interactions between receptors and ligands which are the adhesion sites distributed on a cell and a surface, respectively. A potential bond between a receptor and a ligand may be formed only if the receptor is close enough to the free ligand, which is characterized by the reactive distance d_{on}. A ligand is called free if it is not bound to any receptors. During the time a receptor is within the distance d_{on} to a free ligand, a bond can be formed with on-rate k_{on}. Reversely, existing bonds are ruptured with off-rate k_{off} or if their length exceeds the rupture distance d_{off}. The rates k_{on} and k_{off} are defined as follows

$$k_{on} = k_{on}^0 \exp\left(-\frac{\sigma_{on}(l-l_0)^2}{2k_BT}\right), \qquad k_{off} = k_{off}^0 \exp\left(\frac{\sigma_{off}(l-l_0)^2}{2k_BT}\right), \tag{9}$$

where k_{on}^0 and k_{off}^0 are the reaction rates at the distance $l = l_0$ between a receptor and a ligand with the equilibrium spring length l_0 defined below. The effective on and off strengths σ_{on} and σ_{off} define a decrease or an increase of the corresponding rates within the interaction lengths d_{on} and d_{off}, and k_BT is the unit of energy. The force exerted on the receptors and ligands by an existing bond is given by

$$F(l) = k_s(\tau_w)(l-l_0), \tag{10}$$

where $k_s(\tau_w)$ is the spring parameter; here we will represent it as a linear and non-linear function of the wall-shear-stress (WSS) τ_w. The probabilities of bond formation and dissociation are defined as $P_{on} = 1-\exp(-k_{on}\Delta t)$ and $P_{off} = 1-\exp(-k_{off}\Delta t)$, where Δt is the time step in simulations. This adhesion model is a modification of the well-known adhesive dynamics model developed by Hammer and Apte (10). In their model $\sigma_{on} = \sigma_{ts}$ and $\sigma_{off} = k_s - \sigma_{ts}$, where σ_{ts} is the transition state spring parameter and k_s is a constant.

During the course of a simulation the receptor/ligand interactions are considered every time step. First, all existing bonds between receptors and ligands are checked for a potential dissociation according to the probability P_{off}. A bond is ruptured if $\xi < P_{off}$ and left unchanged otherwise, where ξ is a random variable uniformly distributed on $[0,1]$. If a bond is ruptured the corresponding ligand is available for new binding. Second, all free ligands are examined for possible bond formations. For each free ligand we loop over the receptors within the distance d_{on}, and bond formation is attempted for each found receptor according to the probability P_{on}. This loop is terminated when a bond is formed. Finally, the forces of all remaining bonds are calculated and applied.

Note that this algorithm permits only a single bond per ligand, while receptors may establish several bonds if several ligands are free within their reaction radius. This provides an additional capability for the adhesive dynamics model compared with that employing one-to-one

interactions between receptors and ligands. Also, this assumption appears to furnish a more realistic representation of adhesive interactions of Pf-RBCs with a coated surface. Pf-RBCs display a number of parasitic nanometer-size protrusions or knobs on the membrane surface (11-13), where receptors that mediate RBC adherence are clustered.

Scaling of model and physical units

Scaling between DPD model units (M) and physical units (P) adopts the following length and time scales

$$r^M = \frac{D_0^P}{D_0^M}\, m, \qquad \tau = \frac{D_0^P}{D_0^M}\frac{\eta^P}{\eta^M}\frac{Y_0{}^M}{Y_0{}^P}\, s, \tag{11}$$

where r^M is the model unit of length, D_0 is the cell diameter, m stands for meters, and η is the characteristic viscosity (e.g., internal/external fluids or membrane). Additionally, we can define scaling of the energy per unit mass (k_BT) and of the force unit ("N" denotes Newton) as follows

$$(k_BT)^M = \frac{Y_0{}^P}{Y_0{}^M}\left(\frac{D_0^P}{D_0^M}\right)^2 (k_BT)^P, \qquad N^M = \frac{Y_0{}^P}{Y_0{}^M}\frac{D_0^P}{D_0^M} N^P. \tag{12}$$

In general, there are no limits for the proposed scaling, however close attention has to be paid to the choice of DPD parameters and to the limits of the DPD method. For example, DPD simulations may have a certain limit on the flow velocity due to fluid compressibility (14). Let us select arbitrarily the RBC and fluid properties in model units and calculate the space and time scaling to the corresponding properties in physical units according to equations above. Then, to simulate a flow with some characteristic shear rate in a physical system, we can calculate the shear rate which has to be imposed in the modeled domain according to the scaling. If the shear rate in model units is too high, we may encounter the well-known DPD problems such as fluid compressibility, varying viscosity, and temperature elevation. A proper choice of the DPD parameters (e.g., increase of fluid viscosity, decrease of RBC Young's modulus) will allow us to stay within the limits of the DPD method, where the aforementioned artifacts can be neglected.

MODEL PARAMETERS

Here we present a complete set of model parameters used for the simulations in the paper.

Simulation parameters for the default case

A Pf-RBC is modeled using the stress-free model described above with the following parameters: $\mu_0 = 1000$, $x_0 = 2.2$, $k_a = 50000$, $k_d = 1000$, $k_v = 50000$, and $n = 2$. DPD parameters of interactions among external solvent (S_o), internal fluid (S_i), RBC vertices (V), and wall (W) particles are shown in table 1. Pair interactions which are not specified in table 1 are switched off. The number density of both internal and external fluids is equal to 3. The Schmidt number (*Sc*) of both fluids is equal to 4828, which is close to that of real fluids. Here,

$Sc = \frac{\mu}{\rho D}$, where D is the coefficient of self-diffusion, and $\frac{\mu}{\rho}$ is the kinematic viscosity.

Interaction	a	γ	r_c	$k(DPD\ envelope)$
$S_o - S_o$, $S_o - W$	4.0	10.0	1.5	0.25
$S_i - S_i$	4.0	10.0	1.5	0.25
$S_o - V$, $S_i - V$, $W - V$	2.0	20.0	1.5	0.25
$V - V$	100.0	10.0	0.75	0.25

Table 1: DPD parameters used in the simulations of RBC adhesive dynamics in malaria. Parameters a and γ are the conservative and dissipative force coefficients, r_c is the cutoff radius, and k is the exponent for the DPD envelope.

Initially, an infected RBC is placed between two walls at the distance of 100 nm away from the lower wall. The cell has $N_r = 500$ receptors, while ligands on the lower wall are distributed on the square lattice with lattice constant $d = 0.5$ μm. The shear flow is generated by moving the upper wall. Table 2 presents default simulation parameters in model units and the corresponding physical parameters in SI units.

Parameters	Simulations	Physical
RBC diameter (D_0)	7.82	7.82×10^{-6} m
Young's modulus (Y_0)	3926	16.8×10^{-5} N/m
bending rigidity (k_c)	8.66	3.7×10^{-19} J
shear rate ($\dot{\gamma}$)	0.3333	33.33 s^{-1}
wall shear stress (τ_w)	7.3326	0.317 Pa
temperature (T)	0.1	310 K
external fluid viscosity (η_o)	22	9.5×10^{-3} $Pa\cdot s$
internal fluid viscosity (η_i)	22	9.5×10^{-3} $Pa\cdot s$
spring constant (k_s)	400	1.71×10^{-5} N/m
equilibrium spring length (l_0)	0.0	0.0 m
reactive distance (d_{on})	0.35	3.5×10^{-7} m
rupture distance (d_{off})	0.35	3.5×10^{-7} m
on strength (σ_{on})	1.0	4.28×10^{-8} N/m
off strength (σ_{off})	0.3333	1.43×10^{-8} N/m
unstressed on rate (k_{on}^0)	116.67	11667 s^{-1}
unstressed off rate (k_{off}^0)	1.0	100 s^{-1}
receptor density (n_r)	4.0	4.0 $mol/\mu m^2$
ligand density (n_l)	4.0	4.0 $mol/\mu m^2$

Table 2: Default simulation (in DPD units) and physical (in SI units) parameters for RBC adhesive dynamics in malaria.

The default parameters correspond to the schizont stage of intra-cell parasite development with the Young's modulus approximately ten times larger than that of healthy RBCs.

We verified that relevant physical properties are faithfully represented in our simulations. The fluid viscosity and temperature remain constant for all modeled shear rates, which is mainly achieved through a relatively high fluid viscosity and *Sc* number in comparison with the common DPD parameters (2) which result in both η and *Sc* to be on the order of *O*(1). The compressibility effects are also negligible due to a low fluid velocity next to the cell membrane and the wall, where problems can be expected.

Simulations with varying spring constant

We considered a linear and a non-linear dependence of the spring constant k_s on the wall shear stress (WSS) τ_w. For the linear case k_s is proportional to the WSS as follows

$$k_s(\tau_w) = 54.6\tau_w \text{ (inmodelunits)}, \qquad k_s(\tau_w) = 5.46\times10^{-5}\tau_w \text{ (inSIunits)}. \tag{13}$$

The case of a non-linear dependence of k_s on τ_w is presented in table 3. Initial guess for k_s was guided by the experimental data of Ania et al. (15) assuming linear behavior of k_s and the average flipping velocity with respect to τ_w. However, a second correction for k_s in most of the simulations was necessary, because the dependence of these parameters may be non-linear with respect to τ_w.

τ_w (model units)	3.62	5.84	8.18	11.68	17.53	23.37	29.21
τ_w (Pa)	0.155	0.25	0.35	0.5	0.75	1.0	1.25
k_s (model units)	200	340	460	572	1116	1660	2300
k_s ($\mu N/m$)	8.56	14.55	19.68	24.48	47.76	71.034	98.42

Table 3: Non-linear dependence of k_s on the wall-shear-stress (WSS) τ_w.

Simulations with explicit parasite modeling

The parasite was modeled by a collection of DPD particles within the cylindrical volume with $R = 3.3\ \mu m$ and $L = 0.2\ \mu m$. These particles were placed inside the Pf-RBC and constrained to undergo rigid motion. In order to prevent the parasite body from crossing the RBC membrane, we introduce Lennard-Jones interactions between the parasite body particles and membrane

vertices given by the potential

$$U(r) = 4\varepsilon\left[\left(\frac{\sigma_{MD}}{r}\right)^{12} - \left(\frac{\sigma_{MD}}{r}\right)^{6}\right], \tag{14}$$

where ε and σ_{MD} are energy and length characteristic parameters, respectively. These parameters were set to $\varepsilon = 1.0$ and $\sigma_{MD} = 0.5$. The parasite was allowed to swim freely in the RBC cytosol, while the number of DPD particles that represents the RBC cytosol was reduced according to the volume occupied by the parasite body. The simulation parameters for the membrane and adhesive interactions were the same as in table 2.

RESULTS AND DISCUSSION

Adhesive dynamics of Pf-RBCs on mammalian CHO cells

Antia et al. (15) examined adhesive dynamics of Pf-RBCs on a surface covered with grown mammalian CHO cells. Most of the infected RBCs showed persistent firm adhesion with infrequent complete detachment. This behavior was not attributed to the presence of any other types of ligands, which may be expressed by the mammalian CHO cells, since it is believed that they expose the same ligands as ICAM-1. The flow micro-environment was identified to potentially contribute to the difference in RBC adhesive dynamics on purified ICAM-1 and on mammalian CHO cells.

The adhesive behavior of Pf-RBCs, explored by means of numerical simulations for various parameters, revealed several types of cell dynamics such as firm adhesion, RBC peeling off the surface followed by flipping from its one side to the other or by detachment from the wall, and very slow slipping along the wall. However, the video containing an example of RBC adhesive dynamics on the mammalian CHO cells from experiments (15) shows firm adhesion of Pf-RBCs for some time followed by a sudden detachment. In contrast, firm adhesion in simulations appears to always be stable with no detachment within the simulated time of approximately 30 s. Note that the RBC motion in experiments before the detachment displays very slow slipping along the surface due to the flow and random collisions with other flowing RBCs. Considering the RBC adhesive dynamics observed in simulations and experiments, it is likely that the sudden complete detachment from the wall in this case is caused by RBC slipping into a wall region with a limited number of ligands available for binding.

To verify this hypothesis we ran a simulation in which ligand sites were removed from the wall area between 30 μm and 40 μm in the x direction. RBC slipping along the wall was achieved for the following simulation parameters: $k_c = 1.85\times10^{-18}$ J, $k_s = 3.42\times10^{-6}$ N/m, and $\dot{\gamma} = 6.7$ s^{-1}, while the other parameters were the same as in the default case. Figure presents RBC displacement along the x coordinate (a) and instantaneous velocity (b). show membrane dynamics. This plot illustrates that the membrane surface is much smoother than in the case of low bending rigidity in figure 1 of the paper. High bending rigidity is able to resist stresses exerted by the flow showing no local buckling of the membrane. However, the Pf-RBC experiences strong membrane deformations during the peeling stage of the flipping motion similar to those seen for RBCs with low bending resistance RBC displacement shows a slow slipping along the surface continued up to an x coordinate between 30 μm and 40 μm, where

a complete cell detachment occurs due to no ligands present for binding. The corresponding cell velocity in figure 0b confirms the described dynamics. The simulation results are in good qualitative agreement with the RBC dynamics on the mammalian CHO cells found in experiments (14). At this time, no other change in physical parameters of cell adhesion was found to be able to reproduce this dynamics.

Dependence of RBC adhesive dynamics on membrane bending rigidity

Membrane bending rigidity affects the adhesive dynamics of Pf-RBCs in shear flow. Figure presents several snapshots of a rolling RBC along a wall with the membrane bending rigidity five times larger than that for the default case. This plot illustrates that the membrane surface is much smoother than in the case of the low bending rigidity in figure 1 of the paper. High bending rigidity is able to resist stresses exerted by the flow showing no local buckling of the membrane. However, the Pf-RBC experences strong membrane deformations duriing the peeling stange of the flipping motion similar to those seen for RBCs with low benidng resistance.

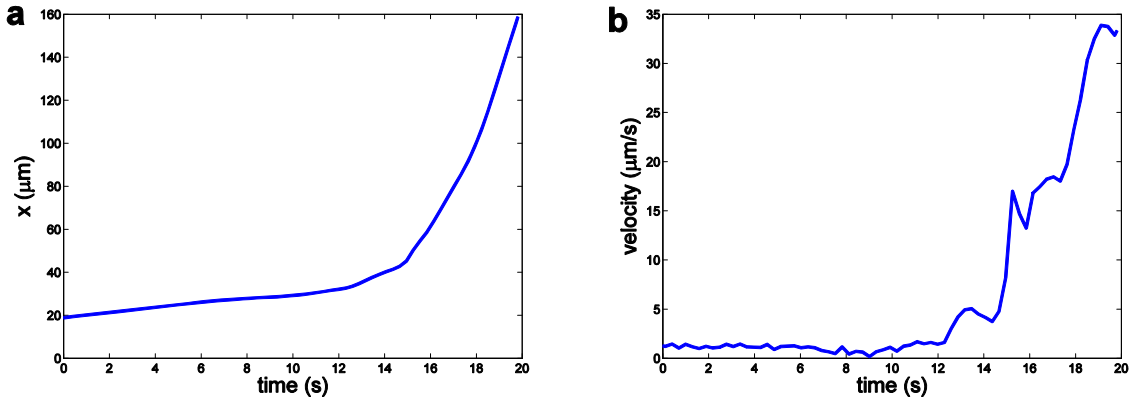

Figure S1: Displacement (a) and velocity (b) of a Pf-RBC along the wall for the case of sudden cell detachment.

MOVIE DESCRIPTION

Movie S1: Adhesive dynamics of a Pf-RBC at the schizont stage with explicit modeling of a parasite. The RBC membrane is partially transparent for visual clarity.
Movie S2: Adhesive dynamics of Pf-RBCs in a microchannel. The lower wall is covered with ICAM-1 but the upper wall is not coated. Healthy RBCs are not shown.

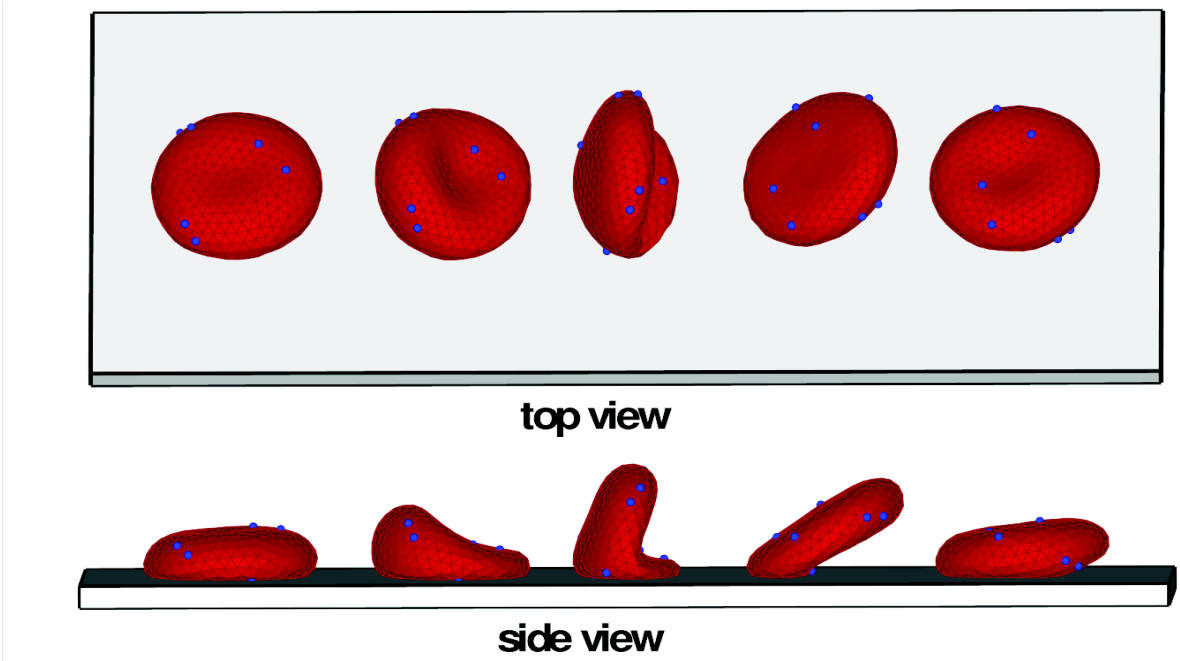

Figure S2: Top and side views of several snapshots of a rolling RBC with the bending rigidity $k_c = 1.85 \times 10^{-18}$ J. Coordinates along the wall for different snapshots are shifted in order to separate them for visual clarity. Blue particles are added as tracers during post-processing to

.

References

[1] Hoogerbrugge, P.J., and J.M.V.A. Koelman, 1992. A. Simulating microscopic hydrodynamic phenomena with dissipative particle dynamics. *Europhysics Letters* 19:155-160.

[2] Groot, R. D., and P. B. Warren, 1997. Dissipative particle dynamics: Bridging the gap between atomistic and mesoscopic simulation. *Journal of Chemical Physics* 107:4423-4435.

[3] Discher, D. E., D. H. Boal, and S. K. Boey, 1998. Simulations of the erythrocyte cytoskeleton at large deformation. II. Micropipette aspiration. *Biophysical Journal* 75:1584-1597.

[4] Fedosov, D. A., B. Caswell, and G. E. Karniadakis, 2010. A multiscale red blood cell model with accurate mechanics, rheology, and dynamics. *Biophysical Journal* 98:2215-2225.

[5] Evans, E. A., and R. Skalak, 1980. *Mechanics and thermodynamics of biomembranes*. CRC Press, Inc., Boca Raton, Florida.

[6] Espanol, P. 1998. Fluid particle model. *Physical Review E* 57:2930-2948.

[7] Fedosov, D. A., B. Caswell and G. E. Karniadakis, 2010. Systematic coarse-graining of

spectrin-level red blood cell models. *Computer Methods in Applied Mechanics and Engineering*, 199:1937-1948.

[8] Helfrich, W., 1973. Elastic properties of lipid bilayers: theory and possible experiments. *Z. Naturforschung C* 28:693-703.

[9] Fedosov, D. A. , 2010. Multiscale modeling of blood flow and soft matter. *PhD thesis*, Brown University, USA.

[10] Hammer, D. A., and S. M. Apte, 1992. Simulation of cell rolling and adhesion on surfaces in shear flow: general results and analysis of selectin-mediated neutrophil adhesion. *Biophysical Journal* 63:35-57.

[11] Howard, R. J., 1988. Malarial proteins at the membrane of Plasmodium falciparum-infected erythrocytes and their involvement in cytoadherence to endothelial cells. *Progress in Allergy* 41:98-147.

[12] Ho, M., and , N. J. White, 1999. Molecular mechanisms of cytoadherence in malaria. *American Journal of Physiology* 276:C1231-C1242.

[13] Nagao, E., O. Kaneko, and J. A. Dvorak, 2000. Plasmodium falciparum-infected erythrocytes: qualitative and quantitative analyses of parasite-induced knobs by atomic force microscopy. *Journal of Structural Biology* 130:34-44.

[14] Fedosov, D.A., I.V. Pivkin, and G.E. Karniadkais, 2008. Velcoity Limit in DPD Simulaitons of Wall Bounded Flows, *Journal of Computational Physics* 227:2540:2559.

[15] Antia, M., T. Herricks, and P. K. Rathod, 2007. Microfluidic modeling of cell-cell interactions in malaria pathogenesis. *PLoS Pathogens* 3:939-945.